

Communication

Toward Near-Ground Localization: Modeling and Applications for TOA Ranging Error

Cheng Xu, Jie He, Xiaotong Zhang, Po-Hsuan Tseng, and Shihong Duan

Abstract—Near-ground localization is a special type of localization scenario that is widely considered in both academic and industry. In this communication, with considering the multipath condition in near-ground environments, we conducted field measurements and proposed an antenna height-dependent time of arrival (TOA) ranging error model. Experiment results show that TOA distance measurement errors accord with Gaussian distribution, and its mean and variance are directly related with antenna height and communication distance. Based on the proposed TOA ranging error model, Cramer–Rao lower bound under typical scenarios have been calculated, and localization performance simulation has been studied. The experiment results indicate that the proposed TOA ranging error model has significant theoretical and practical application values.

Index Terms—Cramer–Rao lower bound (CRLB), multipath, near ground, ranging error, time of arrival (TOA).

I. INTRODUCTION

As a basic attribute of an object, the location information is becoming increasingly important to wireless personal area network (WPAN). Although the global navigation satellite system (GNSS) [1] only requires one local node, it may be out of use in indoor, underground, or dense-constructed areas [1]. Even in outdoor open area, the GNSS is limited by its volume, power consumption, and cost. However, time of arrival (TOA)-based RF localization is an effectively complementary solution, in both indoor and outdoor conditions [2]–[6], since it can be easily deployed and achieve much higher accuracy than the GNSS. With the quickly decreasing of the cost of RF modules, using TOA to localize WPAN nodes is becoming a new trend.

Near ground is a particular application scenario of the TOA-based localization system. Typical examples include near-ground swarm robots used in military, near-ground wireless sensor networks used in agriculture monitoring, landslides monitoring, and volcanic eruption monitoring. The most significant difference between near-ground and common application scenarios is that the antennas are often quite close to the ground and sometimes even just on the ground. For example, the antenna used in a self-healing minefield system [2] was fixed at 7 cm above the ground. The characteristics of near-ground wireless channel have already attracted the attentions of

researchers [2]–[6]. However, these studies mostly focused on the path loss or received signal strength indicator (RSSI) modeling, while the TOA ranging error model has often been neglected.

The TOA ranging error model is widely used to calculate Cramer–Rao lower bound (CRLB) [4], design localization algorithms [6], and simulate the performance of localization systems [4]. However, a ranging error model for near-ground TOA applications is rarely considered among latest literatures. Field experiments on TOA ranging were implemented by Joshi *et al.* [5] in 11 typical indoor and outdoor scenes, with antennas fixed at 15 cm above the earth. Such results helped understand the ranging error for near-ground applications but its generality and flexibility were limited due to the fixed antenna height. Further studies were carried out by Wang *et al.* [7], focusing on antenna heights of 15, 30, and 100 cm above the ground. However, existing studies are mostly focused on the relationship between RSSI and ranging error in near-ground applications, while the TOA-based ranging is rarely studied. Since TOA-based localization is widely used for accurate localization [2]–[6], it is essential and urgent to come up with a height-dependent TOA ranging error model for near-ground applications.

In this communication, field experiments are conducted using the IEEE 802.15.4a chirp spread spectrum-based TOA nodes. The proposed height-dependent TOA ranging error model fits for Gaussian distribution whose mean and variance are related with antenna height and communication distance.

II. MULTIPATH CONDITIONS IN NEAR-GROUND TOA RANGING

In a TOA distance measuring system, the intervening distance is usually obtained by detecting the time of flight of the direct path (DP) between target node (TN) and reference node (RN). However, in multipath environment, RNs may receive a series of signals. DP and reflected paths are mixed together. The combination of these paths contributes to the shift of transmitted waveform. As shown in Fig. 1, with a finite bandwidth, the combination among DP and its nearby paths shifts the peak of DP pulse, resulting in ranging errors.

In near-ground scenarios, multipath conditions are officially defined and described in the standard IEEE Std 211–1997 [8]. According to [8] and [9], the multipath condition is directly related with the height of the node (h) and the distance between TN and RN (d). As shown in Fig. 2, Norton has presented in [9] that the near-ground transmitted wave could be classified into three components, namely directed wave, ground-reflected wave, and surface wave. For a dipole antenna located at h above the ground, the generated magnitude of the electric field could be demonstrated as

$$E_{\text{total}} = \frac{E_0}{d} \left[\underbrace{\cos^3(\phi_0)e^{-\gamma_0 R_0}}_{\text{Direct Wave}} + \underbrace{\Gamma_{v,h} \cos^3(\phi_1)e^{-\gamma_0 R_1}}_{\text{Ground-reflected Wave}} + \underbrace{(1 - \Gamma_{v,h})F(\omega) \cos^2(\phi_1)e^{-\gamma_0 R_1}}_{\text{Surface wave}} \right] \quad (1)$$

Manuscript received August 18, 2016; revised June 25, 2017; accepted August 10, 2017. Date of publication August 21, 2017; date of current version October 5, 2017. This work was supported in part by the National Natural Science Foundation of China under Project 61671056, Project 61302065, and Project 61304257, in part by the Natural Science Foundation of Beijing Municipality under Grant 4152036, and in part by the Fundamental Research Funds for the Central Universities under Grant FRF-TP-15-026A2. (Cheng Xu and Jie He are co-first authors.) (Cheng Xu and Jie He contributed equally to this work.) (Corresponding authors: Jie He; Po-Hsuan Tseng.)

C. Xu, J. He, X. Zhang, and S. Duan are with the School of Computer and Communication Engineering, University of Science and Technology Beijing, Beijing 100083, China (e-mail: hejie@ustb.edu.cn; phtseng@ntut.edu.tw).

P.-H. Tseng is with the Beijing Key Laboratory of Knowledge Engineering for Materials Science, Department of Electronic Engineering, National Taipei University of Technology, Taipei 10608, Taiwan.

Color versions of one or more of the figures in this communication are available online at <http://ieeexplore.ieee.org>.

Digital Object Identifier 10.1109/TAP.2017.2742551

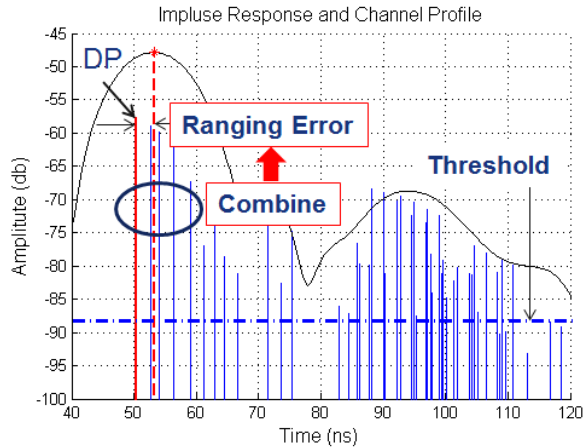


Fig. 1. Channel response of near-ground wireless channel in time domain. The combination among DP and its nearby paths shift the peak of DP pulse, resulting in ranging errors.

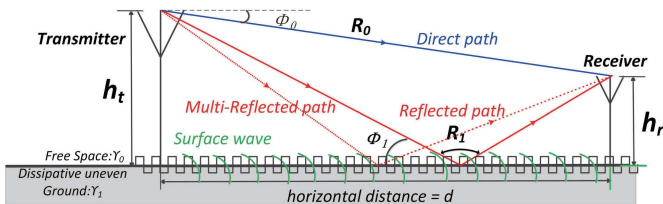


Fig. 2. Multipath condition of near-ground wireless channel: a sketch of typical near-ground scenario. TN and RN antennas are put on top of a dielectric half-space, showing direct waves, ground-reflected waves, and surface waves.

where E_0 is a reference value representing the excitation and $\Gamma_{v,h}$ is the Fresnel plane-wave reflection coefficient of the boundary between the free space and the dissipative ground for vertical and horizontal antenna polarization. γ_0 is the dielectric medium of free space. $F(\omega)$ denotes the Sommerfeld attenuation function. R_0 , R_1 , ϕ_0 , ϕ_1 , and h are defined in Fig. 2. More information please refer to [9].

It can be seen that the near-ground transmitted wave is related with antenna height h and communication distance d . They are usually used to analyze or model the characteristics of path loss in near-ground scenarios [4]–[6]. However, to the best of our known, TOA ranging error has seldom been studied. It is necessary to give full consideration to different influence factors of near-ground TOA transmission. Thus, we focus on the factors of d and h , conduct field experiments, and propose a TOA ranging error model for near-ground applications.

III. TOA RANGING MEASUREMENTS

Practical distance measurements are performed in outdoor area, using commercially available TOA-based localization system. Statistics of the distance measurement errors (DMEs) are used to model the influences of antenna height and communication distance on near-ground TOA ranging accuracy.

A. Scenario Settings

As shown in Fig. 3(a), the devices used for measurements are designed based on NanoLOC, an RF chip with the capability of TOA measurement, running on the IEEE 802.15.4a Standard. It is mainly composed of the following components: a 32 b RISC instruction set ARM processor (STM32F103), a NanoLOC RF chip (working at a frequency of 2.4 GHz), an RF front-end CC2591, and a typical 3-dBi gain rod antenna [shown in Fig. 3(b)]. NanoLOC performs the TOA

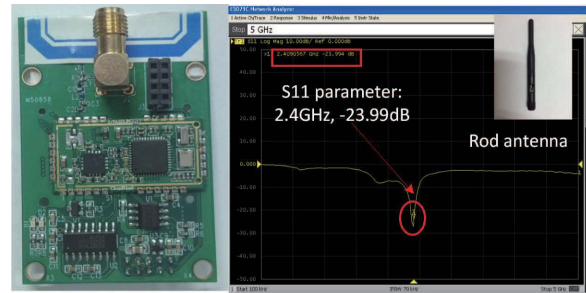


Fig. 3. (a) Hardware design is demonstrated. (b) S11 parameter is displayed together with the rod antenna used in our measurement.

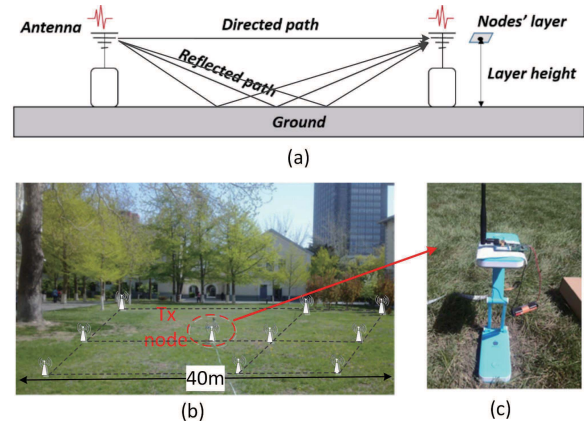


Fig. 4. Measurement scenario for near-ground TOA ranging. (a) Schematic of the testing scenario. (b) Field testing scenario. (c) Schematic of antenna placement.

ranging algorithm in both directions (namely TWR ranging) [10]. The transmission packets contain timestamps, which are used to synchronize TN and RN. No external synchronization mechanisms are needed [10]. The antenna frequency response is measured by an Agilent Network Analyzer, as shown in Fig. 3(b).

The measurement was conducted in an open field of the University of Science and Technology Beijing. Two nodes are set to be RN and TN, respectively. TN and RN are placed, respectively, on a lifttable support, fixed at the same height. A schematic of the testing scenario is displayed in Fig. 4(a) and (c). Therefore, measurements conducted in this communication cover various h and d values, to analyze the impacts of these factors on TOA ranging error. A measuring case set is as follows:

$$\text{Case} = \{h, d\}. \quad (2)$$

Settings of h and d are shown in Table I. Values of h include 0, 2, 4, 6, 8, 10, 15, and 20 cm. A specific case can be Case = {6 cm, 20 m}. For each case, DME, denoted as $\epsilon_h(d)$, is considered. DME is modeled with antenna height and TN-RN distance, and it could be defined as $\epsilon_h(d) = \hat{d}_h - d$. \hat{d}_h is the ranging result when an antenna is fixed at height h , and RN is placed d away from TN. Up to 10000 cases are collected in each condition, to validate the typicalness and transferability.

B. Modeling Near-Ground TOA Ranging

A statistical model on DME is put forward in order to better quantitatively analyze TOA ranging error under near-ground condition. By examining large amounts of field measuring outcomes, compared with several common distributions, such as Rayleigh, Gamma, Log-normal, and so on, we find DME is more likely consistent with

TABLE I
SETTINGS OF TOA MEASUREMENT

h (cm)	d (m)
0	{1,2,3,4,5,6,7,8,9,10,15,20,21,22}
2	{1,2,3,4,5,6,7,8,9,10,15,20,22,23,24}
4	{1,2,3,4,5,6,7,8,9,10,15,20,25,26,27}
6	{1,2,3,4,5,6,7,8,9,10,15,20,25,27,28,29}
8	{1,2,3,4,5,6,7,8,9,10,15,20,25,29,30,31}
10	{1,2,3,4,5,6,7,8,9,10,15,20,25,30,32,33,34}
15	{1,2,3,4,5,6,7,8,9,10,15,20,25,30,35,38,39,40}
20	{1,2,3,4,5,6,7,8,9,10,15,20,25,30,35,40,44,45,46}

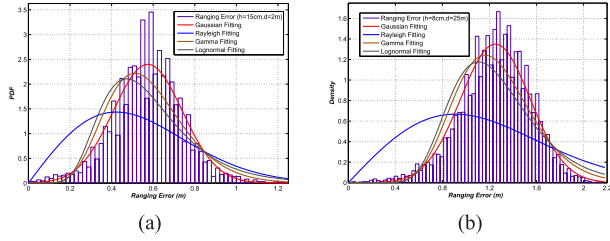


Fig. 5. MATLAB fitting results for near-ground TOA ranging error. Fitting curves for Gaussian, Rayleigh, Gamma, and Lognormal distribution are demonstrated. (a) $h = 15$ cm and $d = 2$ m. (b) $h = 8$ cm and $d = 25$ m.

Gaussian distribution, namely

$$\epsilon_h(d) \sim \mathcal{N}(\mu_{d,h}, \sigma_{d,h}^2) \quad (3)$$

where $\mu_{d,h}$ and $\sigma_{d,h}^2$ denote the mean and variance, respectively. DME distribution for typical measurement cases has been shown in Fig. 5. It is worth mentioning that both $\mu_{d,h}$ and $\sigma_{d,h}^2$ have direct relationship with the antenna height h and TN-RN distance d .

According to the investigation results of experimental data, under the condition of the given ground height h , the mean value of ranging error Gaussian distribution $\mu_{d,h}$ and the actual distance between nodes d can be mathematically modeled as a linear function, namely

$$\mu_{d,h} = a_h \times d + b_h \quad (4)$$

where a_h and b_h are parameters related with corresponding antenna height h . Furthermore, fitting results for $\mu_{d,h}$ have been demonstrated in Fig. 6.

Making use of a_h and b_h under various h values, statistical model between a_h , b_h , and antenna height could be achieved

$$\begin{cases} a_h = -0.002614 \times h + 0.0764 \\ b_h = -0.008753 \times h + 0.6456. \end{cases} \quad (5)$$

The fitting results for a_h and b_h are shown in Fig. 7, and $\mu_{d,h}$ can be described as

$$\begin{aligned} \mu_{d,h} &= a_h \times d + b_h \\ &= (-0.002614 \times h + 0.0764) \times d - 0.008753 \times h + 0.6456. \end{aligned} \quad (6)$$

Similarly, curve fitting approach can be applied to $\sigma_{d,h}^2$. However, under the condition of certain antenna height h , the relationship between ranging error variance $\sigma_{d,h}^2$ and actual TN-RN distance d is approximately in accordance with logarithmic function. Fitting result for $\sigma_{d,h}^2$ is as follows:

$$\sigma_{d,h}^2 = c_h \times \log(f_h \times d + 1) \quad (7)$$

where c_h and f_h are parameters related with antenna height h . Fitting results are described in Fig. 8. We also model c_h and f_h as patters

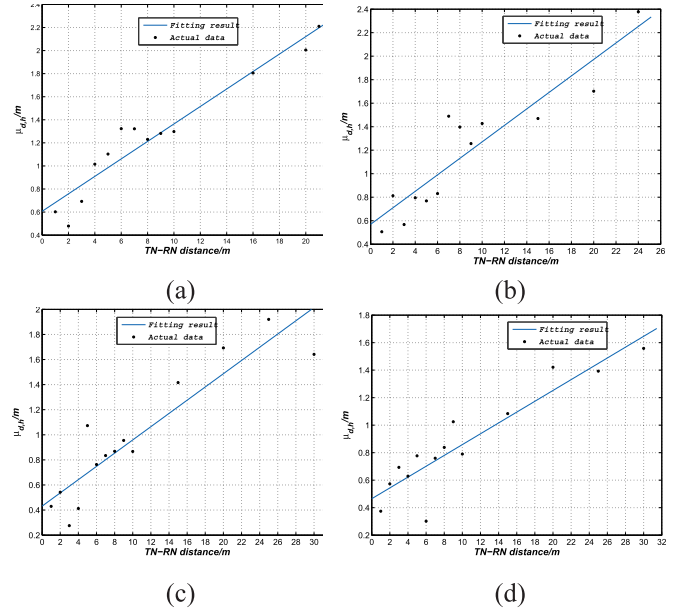


Fig. 6. Curve fitting result for height-dependent coefficients a_h and b_h . (a) Curve fitting for $h = 0$ cm. (b) Curve fitting for $h = 4$ cm. (c) Curve fitting for $h = 8$ cm. (d) Curve fitting for $h = 15$ cm.

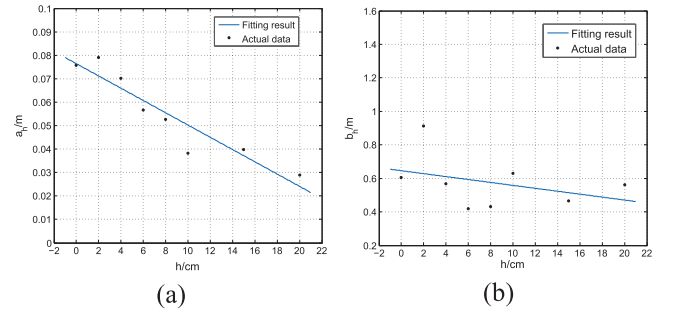


Fig. 7. Curve fitting result for height-dependent coefficients a_h and b_h . (a) Curve fitting for a_h . (b) Curve fitting for b_h .

on antenna height h , and the fitting results are

$$\begin{cases} c_h = c_0 = 0.08981 \\ f_h = -0.09114 \times h + 1.838. \end{cases} \quad (8)$$

The fitting results for c_0 and f_h are in Fig. 9, which shows that c_h has nothing related with antenna height. Similarly, $\sigma_{d,h}^2$ is

$$\begin{aligned} \sigma_{d,h}^2 &= c_0 \times \log(f_h \times d + 1) \\ &= 0.08981 \times \log[(-0.09114 \times h + 1.838) \times d + 1]. \end{aligned} \quad (9)$$

All above, the near-ground TOA ranging error could be modeled as

$$\epsilon_h(d) \sim \mathcal{N}(\mu_{d,h}, \sigma_{d,h}^2) \quad (10)$$

where $\mu_{d,h}$ and $\sigma_{d,h}^2$ are given in (22) and (25).

For verifying the validity of the model, representative measurement results are compared with model generating results. As shown in Fig. 10, when TN and RN antennas are placed at 6 cm away off the Earth, and TN-RN distance is selected as {1, 4, 7, 10, 15, 20, 25, 28 m}, the simulated ranging error has a high concordance with the field measurement results.

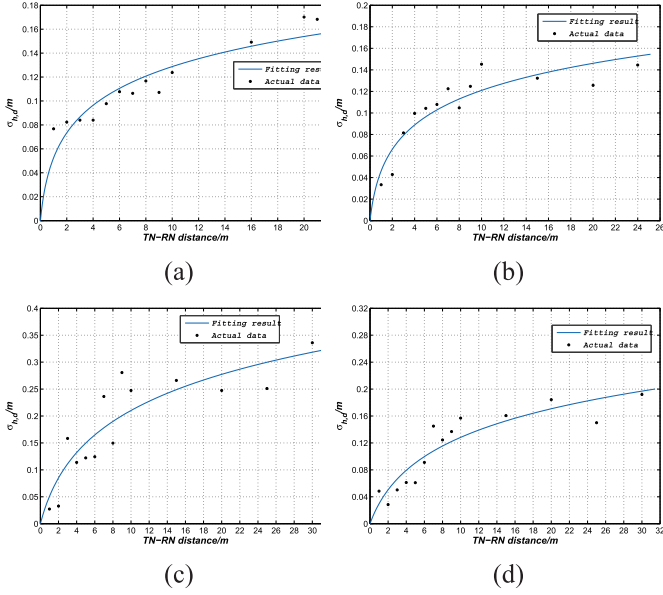


Fig. 8. Curve fitting result for height-dependent coefficients c_h and f_h . (a) Curve fitting for $h = 0$ cm. (b) Curve fitting for $h = 4$ cm. (c) Curve fitting for $h = 8$ cm. (d) Curve fitting for $h = 15$ cm.

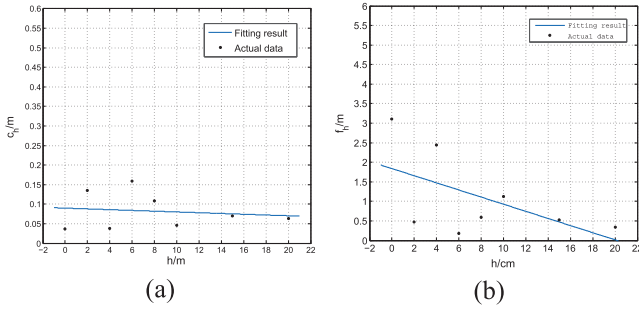


Fig. 9. Curve fitting result for height-dependent coefficients c_h and f_h . (a) Curve fitting for c_h . (b) Curve fitting for f_h .

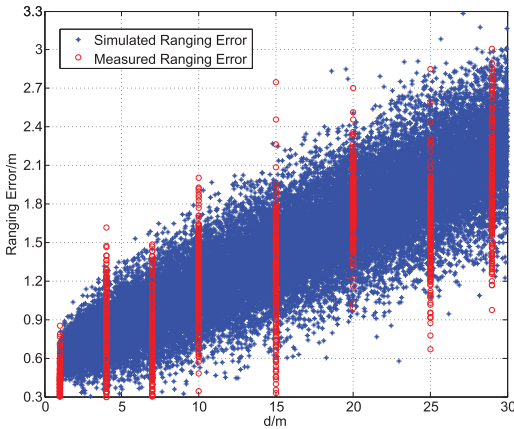


Fig. 10. Validation for the proposed near-ground TOA ranging error model, $h = 6$ cm, and d varies from 1 to 28 m.

IV. TYPICAL USE CASES AND DISCUSSION

The most significant applications of the TOA ranging error model are to calculate CRLB and simulate the performance of localization systems. We represent two typical use cases: absolute localization and relative localization in the same scenario shown in Fig. 4. Furthermore, the measurement setup is described in Figs. 4(b) and 11.

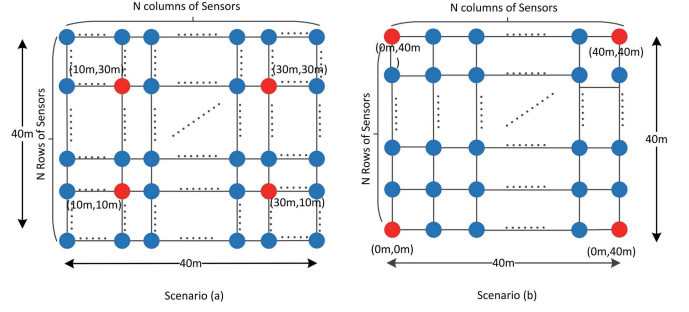


Fig. 11. Spatial distribution of N^2 nodes in constrained system, with four RNs and $(N^2 - 4)$ TNs.

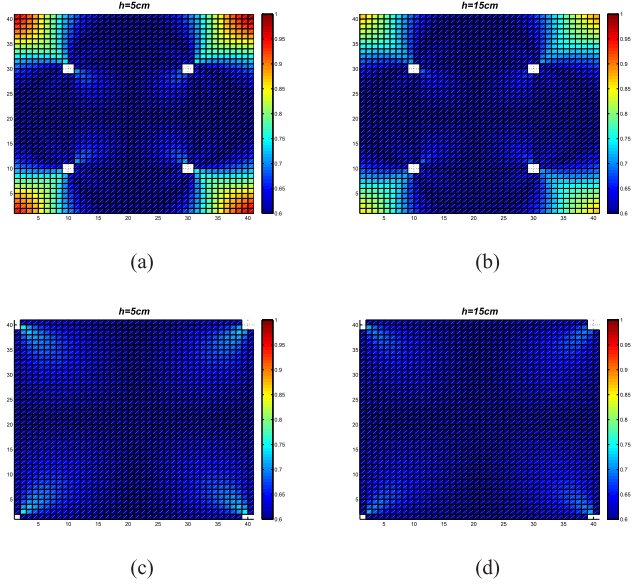


Fig. 12. CRLB calculation for absolute localization in two map configurations. (a) and (b) Under Scenario a). (c) and (d) Under Scenario b).

A. Constrained System

Absolute localization is performed between TNs and location-aware RNs. Only TN-RN ranging distance is mattered for positioning results. A $40\text{ m} \times 40\text{ m}$ square experimental place with plane ground is selected, as shown in Fig. 4(b). Totally 41×41 nodes are deployed evenly with four fixed RNs and $N^2 - 4$ TNs. In Fig. 11(a), RNs are located at $(10\text{ m}, 10\text{ m})$, $(10\text{ m}, 30\text{ m})$, $(30\text{ m}, 10\text{ m})$, and $(30\text{ m}, 30\text{ m})$, and target points are located alongside the outer ring of the region every 1 m. In Fig. 11(b), the four RNs are located at $(0\text{ m}, 0\text{ m})$, $(0\text{ m}, 40\text{ m})$, $(40\text{ m}, 0\text{ m})$, and $(40\text{ m}, 40\text{ m})$, and target points are located alongside the inner ring of the region every 1 m. For *two typical heights 5 and 15 cm* in these two map configurations, CRLB is considered.

However, *relative localization*, namely cooperative localization, utilizes only location-unknown TNs in the system. N nodes are placed inside the experimental region, while N is selected as 4, 7, 11, and 15. Antenna heights h range from 5 to 20 cm, and experiments are conducted every 1 cm. CRLB under each condition (denoted as $\text{CRLB}_{N \times N}$) is calculated and demonstrated as follows.

B. Theoretical Use Case: CRLB Simulation Results

With four location-aware RNs placed, CRLB results under two locating scenarios toward near-ground TOA positioning are achieved, as shown in Fig. 12.

1) *Absolute Localization Performance*: Fig. 12(a) and (b) shows CRLB distribution of Scenario a) where RNs are located within the

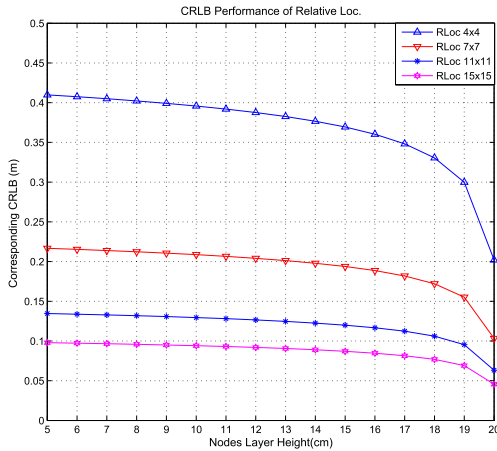


Fig. 13. Nodes average CRLB varies with corresponding layer height under different distributed densities in relative localization.

region. Fig. 12(c) and (d) shows CRLB with RNs located in the corner of region, namely Scenario b). With close observation, following results could be achieved.

- 1) With antenna placed lower, CRLB increases, which reveals larger bounds and worse estimation performance. This also implies that TOA ranging error may become larger with lower antenna heights.
- 2) Localization performance is sensitive to relative positions between antennas. The region corners show worse performance. Positions alongside the diagonal are also worse than others. Taking $h = 15$ cm for example, CRLB of all positions are beneath 0.9 m^2 , however, parts of which show superior performance under 0.7 m^2 .
- 3) Moreover, different RN positions result in different CRLB distributions. When RNs are located in the outer corner of the located area, CRLB is obviously less than those when RNs are located in the inner side.

2) *Relative Localization Performance*: Under various antenna heights, node density is considered, and results are demonstrated in Fig. 13. It shows that taking $h = 20$ cm for example, $\text{CRLB}_{15 \times 15} < \text{CRLB}_{11 \times 11} < \text{CRLB}_{7 \times 7} < \text{CRLB}_{4 \times 4}$, and the performance is maintained at other antenna heights. Besides, CRLB becomes smaller as nodes density rises, namely larger density contributes to better performance.

C. Practical Use Case: Localization Performance Simulation

The TOA ranging error model also has important practical value in simulating the performance of localization systems. In this section, we evaluate three most generally used localization algorithms, namely *centroid localization*, *maximum likelihood localization*, and *Taylor series expansion localization*. Similar to those shown in Fig. 11, two simulation scenarios are considered, with RNs are located in the inner or outer edges of the localization area. For accuracy representation, root mean squared error (RMSE) is calculated and denoted as

$$\text{MSE} = \sqrt{\frac{\varepsilon_1^2 + \varepsilon_2^2 + \dots + \varepsilon_n^2}{n}} = \sqrt{\frac{\sum_{i=1}^n \varepsilon_i^2}{n}} \quad (11)$$

where ε_i is the localization error at each sample point and n is the sampling number. The higher performance some positioning algorithm has, the closer MSE is to CRLB.

Traditional CRLB calculation is aiming at unbiased estimation, such as in [4]. However, the model proposed in this communication indicates that near-ground TOA ranging error conforms to biased estimation [11], namely systematic error exists. A simple improved

TABLE II
SIMULATION RESULTS RMSE COMPARED WITH CRLB

RMSE \ Algorithm	Configure	Scenario-(a)		Scenario-(b)	
		without	with	without	with
Centroid		4.3105	1.6313	2.3484	1.3988
Maximum Likelihood		1.4562	0.7517	1.2416	0.6808
Taylor Series Expansion		1.7389	0.7135	1.2202	0.6985
CRLB_{ave}		0.6097		0.6134	

method is to minus the mean of estimated error from the ranging value. Results with or without using this method are demonstrated in Table II.

All these three algorithms perform differently even under the same scenario, reflecting different localization accuracies, especially compared with CRLB. Besides, each of these three algorithms shows different performances under the two conditions, which is validated again that RN position matters. Furthermore, improved unbiased method tends to have lower RMSE estimations, and it is more close to the CRLB derived by the proposed model. Maximum likelihood and Taylor series expansion show better performance under these two scenarios, however, they still have larger RMSE than CRLB, which means that they both have room for improvement.

V. CONCLUSION

In this communication, we conduct field measurements to conclude a statistical TOA ranging error model. Experiment results show that TOA ranging errors accord with Gaussian distribution, and its mean and variance are directly related with antenna height and TN-RN distance. Based on the proposed TOA ranging error model, CRLB under typical scenarios has been calculated, and localization performance simulation has been studied. The results indicate that the proposed TOA ranging error model has significant application values.

REFERENCES

- [1] C. J. Hegarty and E. Chatre, "Evolution of the Global Navigation Satellite System (GNSS)," *Proc. IEEE*, vol. 96, no. 12, pp. 1902–1917, Dec. 2008.
- [2] W. M. Merrill, H. L. N. Liu, J. Leong, K. Sohrabi, and G. J. Pottie, "Quantifying short-range surface-to-surface communications links," *IEEE Antennas Propag. Mag.*, vol. 46, no. 3, pp. 36–46, Jun. 2004.
- [3] M. A. Landolsi *et al.*, "Performance analysis of time-of-arrival mobile positioning in wireless cellular cdma networks," in *Trends in Telecommun. Technol.* Rijeka, Croatia: InTech, Mar. 2010.
- [4] J. Shen, A. F. Molisch, and J. Salmi, "Accurate passive location estimation using TOA measurements," *IEEE Trans. Wireless Commun.*, vol. 11, no. 6, pp. 2182–2192, Jun. 2012.
- [5] G. G. Joshi *et al.*, "Near-ground channel measurements over line-of-sight and forested paths," *IEE Proc.-Microw., Antennas Propag.*, vol. 152, no. 6, pp. 589–596, Dec. 2005.
- [6] G. Bellusci *et al.*, "Modeling distance and bandwidth dependency of TOA-based UWB ranging error for positioning," *J. Electr. Comput. Eng.*, vol. 2009, Feb. 2009, Art. no. 468597.
- [7] D. Wang, L. Song, X. Kong, and Z. Zhang, "Near-ground path loss measurements and modeling for wireless sensor networks at 2.4 GHz," *Int. J. Distrib. Sensor Netw.*, vol. 8, no. 8, p. 969712, Jun. 2012.
- [8] D. Liao and K. Sarabandi, "Near-earth wave propagation characteristics of electric dipole in presence of vegetation or snow layer," *IEEE Trans. Antennas Propag.*, vol. 53, no. 11, pp. 3747–3756, Nov. 2005.
- [9] K. A. Norton, "The calculation of ground-wave field intensity over a finitely conducting spherical earth," *Proc. IRE*, vol. 29, no. 12, pp. 623–639, Dec. 1941.
- [10] (2017). *Nanotron*. [Online]. Available: http://nanotron.com/EN/PR_ic_modules.php
- [11] X. Lin and Y. Bar-Shalom, "Multisensor target tracking performance with bias compensation," *IEEE Trans. Aerosp. Electron. Syst.*, vol. 42, no. 3, pp. 1139–1149, Jul. 2006.